ELSEVIER

Journal of Marine Systems 20 (1999) 357–379

JOURNAL OF MARINE SYSTEMS

# A seasonal three-dimensional study of the nitrogen cycle in the Mediterranean Sea: Part II. Verification of the energy constrained trophic model

G. Crispi *, A. Crise, E. Mauri

*Osservatorio Geofisico Sperimentale, P.O. Box 2011, 34016 Trieste, Italy*

Received 5 November 1996; accepted 24 September 1997

**Abstract**

In this study the lower trophic level variability induced by physical forcings in the Mediterranean is investigated by means of a three-dimensional coupled hydrodynamical–ecological model, where the lower trophic dynamics are described using an NPD aggregated model. The seasonal cycle of the ecosystem response shows marked spatial differences according to the prevailing cyclonic or anticyclonic regimes and to the zonal and meridional permanent trophic gradients. The interplay between the mixed layer dynamics and the irradiance penetration explains the gross ecosystem vertical dynamics while the general circulation contributes to establish the prevailing trophic regime in the sub-basins. Comparison of simulated chlorophyll concentrations with corresponding CZCS images shows remarkable similarities both in gradients and fields in different seasons. The main spatial characteristics of the seasonal biochemical cycles are resolved with the proposed approach. Moreover the orders of magnitude of obtained results, both for the inorganic nitrogen evolution and for the phytoplankton growth, are in keeping with the data considered. The main conclusion is that even a simplified trophodynamic model coupled with open sea hydrodynamics can satisfactory reproduce the main basin scale features and their seasonal evolution when the first trophic level is energy limited. 

*Keywords:* nitrogen; Mediterranean Sea; trophic model

## 1. Introduction

The Mediterranean semi-enclosed basin is characterized by ‘concentration’ processes, driven by the combined action of the excess of evaporation over precipitation and river runoffs, and a slight heat loss (Garrett, 1994), and it is considered to be the largest oligotrophic area in the world.

These two processes are strictly related: the estuarine inverse circulation directly driven by thermohaline forcings generates a negative budget for nutrients at the Gibraltar Strait. Here the nutrient export in the deep layer exceeds the import (Coste et al., 1988), even though the Surface Atlantic Water transports nutrients into the nutrient-depleted surface mediterranean waters.

This permanent trophic deficit must be balanced on a basin-wide scale by other independent sources,

* Corresponding author. Tel.: +39-040-214-0205; Fax: +39-040-327307; E-mail: gcrispi@ogs.trieste.it

0924-7963/99/$ - see front matter 
PII: S0924-7963(98)00085-2

such as nitrogen fixation (Béthoux and Copin-Montegut, 1986), atmospheric inputs (Duce, 1986; Alarçon and Cruzado, 1989) and riverine inputs (Aleem and Dowidar, 1967). However oligotrophy is not found always and everywhere: mesotrophic conditions seem to develop seasonally in coastal areas where deepening of mixed layer, wind-driven upwellings and riverine inputs mitigate the chronic lack of nutrients in the productive layer. The shelf/open ocean exchanges do not seem very effective in the Mediterranean because the only well developed shelf is along the Provençal and Catalan coasts. Exchanges with the marginal seas, the Adriatic and Aegean, are presently still under evaluation (Civitarese et al., 1995; Poulain et al., 1996).

Although the gross phenomenology of the seasonal trophic dynamics can be assessed, much greater difficulties are found in developing an analogue for the biological dynamics.

Available data for the western Mediterranean ecosystem are mainly regional and, in particular, few observations are at our disposal for the open sea. Studied regions are the Catalan Sea (Cruzado, 1984; Estrada and Margalef, 1988), the Gulf of Naples (Carrada et al., 1980), the Alboran Sea (Prieur and Sournia, 1994) and the northwestern Mediterranean Sea (Martin and Barth, 1995).

Observations of elevated chlorophyll-*a* concentrations, related to coastal upwelling and mesoscale features in the western basin, indicate the need for a reassessment of the Mediterranean trophic characteristics, at least in specific areas (Jacques, 1989).

In the eastern Mediterranean, the Cyprus Gyre (Krom et al., 1991, 1992), the northeastern Mediterranean (Salihoglu et al., 1990; Yilmaz et al., 1994) and the southeastern Mediterranean (Yacobi et al., 1995) are affected by the influence of the cyclonic and anticyclonic patterns present in those areas, which strongly perturb the typical oligotrophic regime of the Levantine Basin.

Complementing these regional studies, more ambitious ongoing international efforts are converging on multidisciplinary collaborative basin-wide programs like those sponsored by the EC Mediterranean Targeted Projects (for an overview see Canals and Lipiatou, 1994; Wassman and Tselepides, 1995), and the POEM-BC surveys in the eastern Mediterranean (Roether et al., 1996).

Only recently mesoscale process studies in regional areas, based on a three-dimensional numerical simulations, were proposed (Pinazo et al., 1996; Zavatarelli and Baretta, 1996).

The quest for an overall three-dimensional representation of Mediterranean biogeochemical processes, as that proposed in the present paper, is multifaceted.

Firstly, a good resolution of the cyclonically induced vertical upwellings in the surface layer is necessary to treat the biology in sufficient detail to capture the seasonal response (Jamart et al., 1979). Moreover, the physical model must also take into account the deep convective mixed layers present in some seasons and the subsequent switch of this regime to stratification.

Secondly the remineralization of the particulate and organic matter must be followed in great detail at the sub-basin scale to obtain the total balance of nutrients at the global scale (Sarmiento et al., 1993). The transformation processes of the biogenic material in the water column have typical time scales of the same order (or longer) as those typical of the general circulation, so the pathways and the ultimate fate of what is exported from the productive layer are strongly influenced by the transport and diffusion dynamics.

The third reason is that a thorough ecosystem study cannot be reduced to a water-column dynamics. Horizontally driven processes, such as upwellings, subduction, fronts, transient and permanent gyres strongly affect the biological dynamics, giving access to biogeochemical energy and decoupling bioprovinces.

This work takes into account both the biochemical and hydrodynamical aspects, by studying the abovementioned interactions in the framework of a primitive equation general circulation model.

A numerical implementation of the model's three-dimensional analytical formulation for the trophic seasonal cycle in the Mediterranean Sea was presented in a companion paper (Crise et al., 1998). The coupling with an Ocean General Circulation Model, able to reproduce the main patterns of the general circulation (Pinardi et al., 1993) as well as the variability of the water mass fluxes at the principal straits (Roussenov et al., 1995; Wu and Haines, 1996), gave an insight in the upper Mediter-

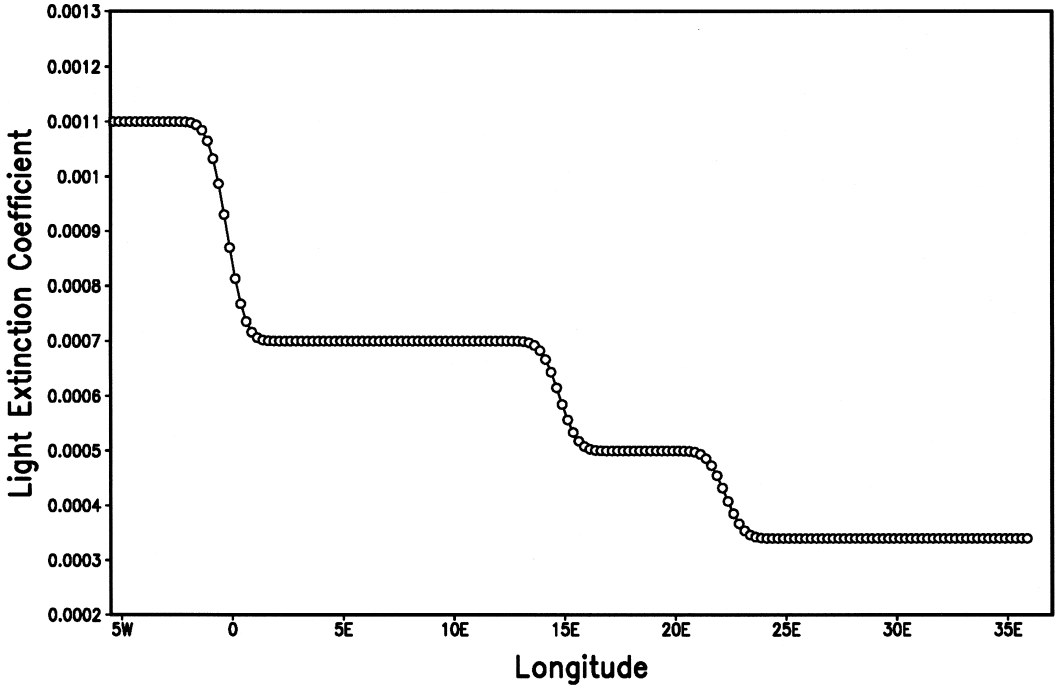


Fig. 1. Light extinction coefficient $k_z$ ($cm^{-1}$) used in the model vs. longitude.

ranean biochemical components distributions and dynamics.

In this paper the nutrients and phytoplankton dynamics will be analyzed in areas where in situ data

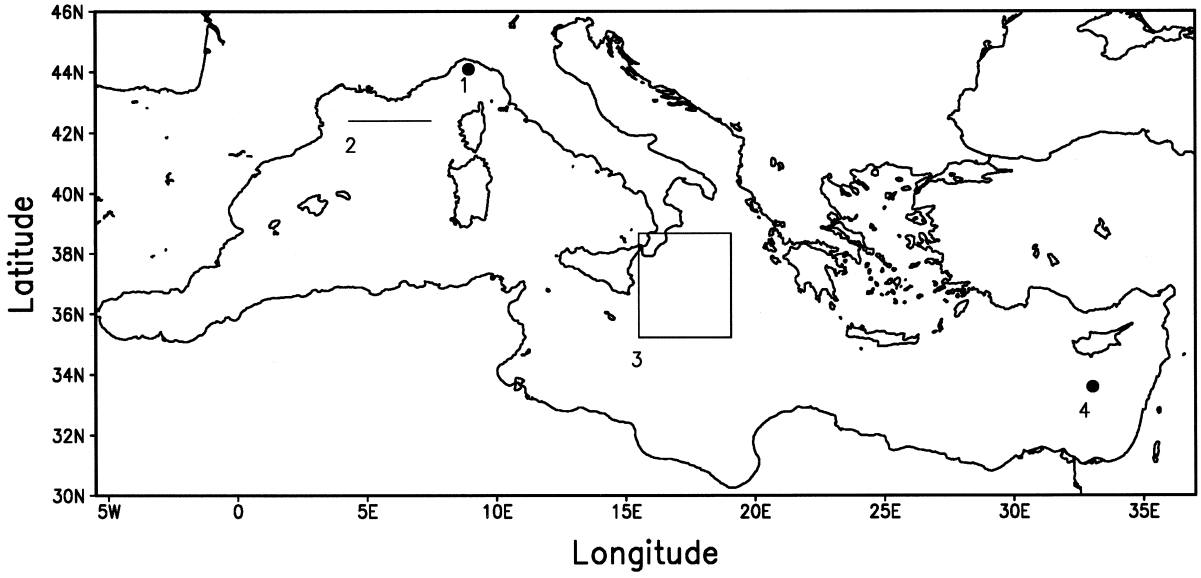


Fig. 2. The stations, transect and area of the model compared with data acquired in the following four regions of the Mediterranean Sea: (1) Ligurian Sea (Fabiano et al., 1984); (2) Provençal Sea (Coste et al., 1972; Jacques et al., 1973); (3) Ionian Sea (Rabitti et al., 1994); (4) Levantine Sea (Berman et al., 1986).

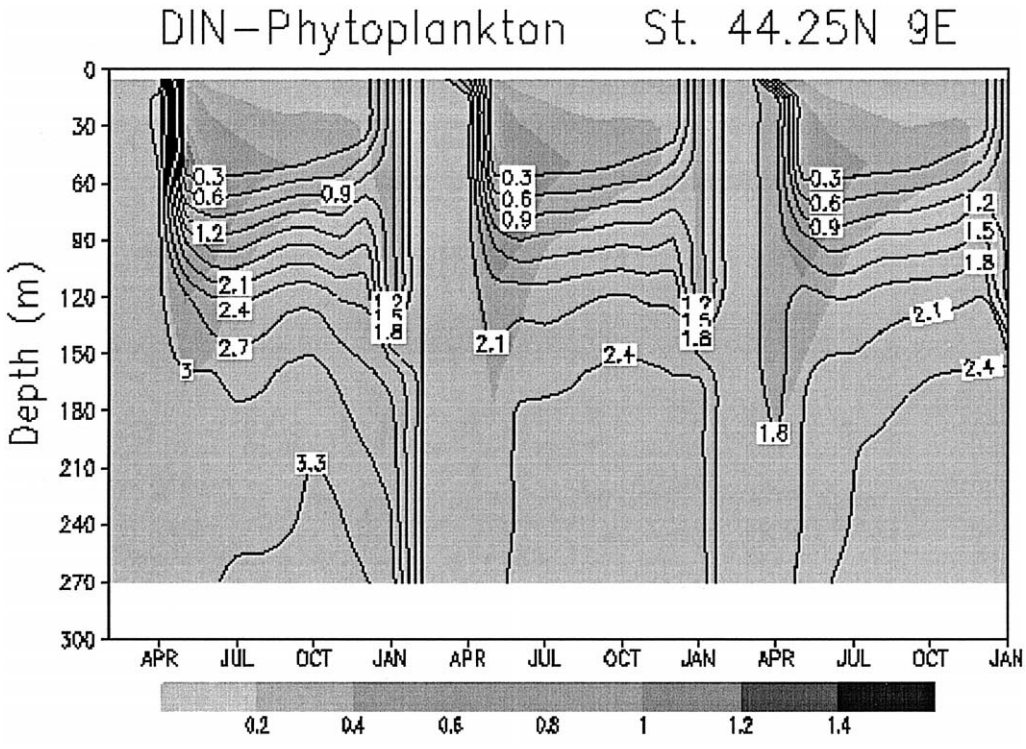
DIN–Phytoplankton St. 44.25N 9E
Depth (m)
0
30
60
90
120
150
180
210
240
270
300
APR JUL OCT JAN APR JUL OCT JAN APR JUL OCT JAN
0.2 0.4 0.6 0.8 1 1.2 1.4

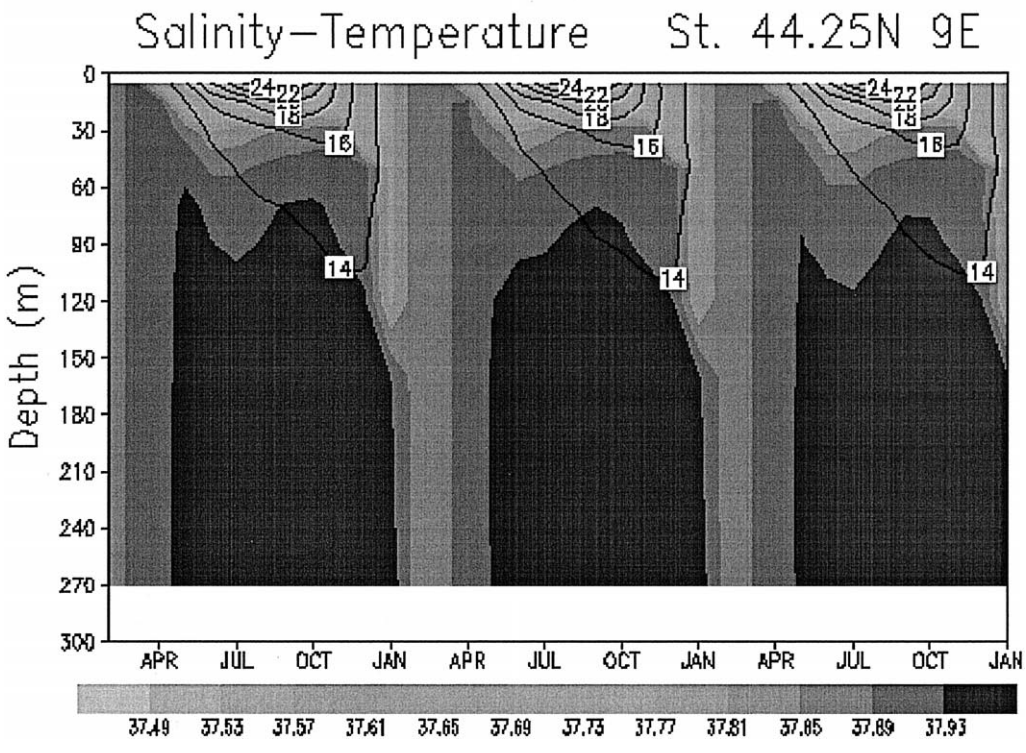
Salinity–Temperature St. 44.25N 9E
Depth (m)
0
30
60
90
120
150
180
210
240
270
300
APR JUL OCT JAN APR JUL OCT JAN APR JUL OCT JAN
37.49 37.53 37.57 37.61 37.65 37.69 37.73 37.77 37.81 37.85 37.89 37.93

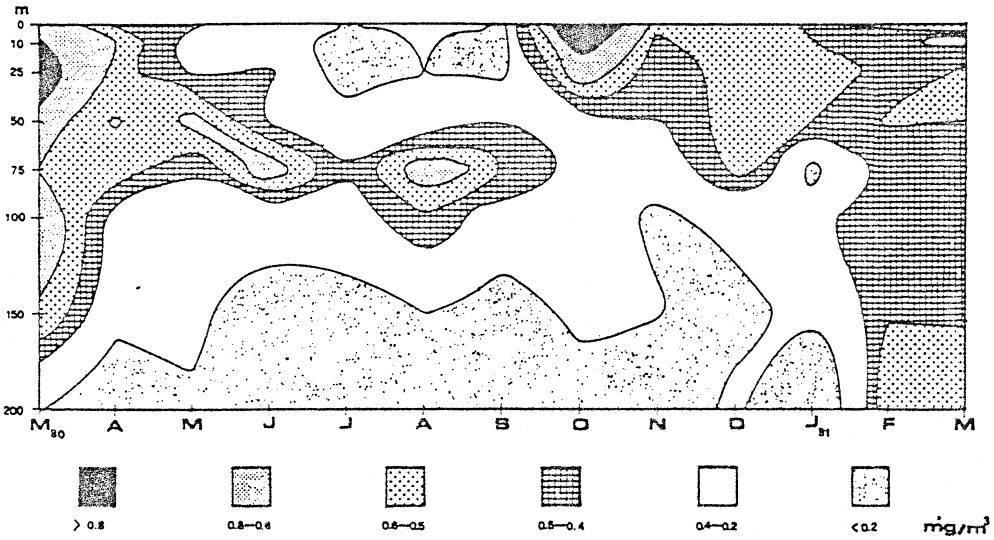


Fig. 4. Annual evolution of the chlorophyll concentrations (mg $m^{-3}$) at station 44.15N 9.13E, after Fabiano et al. (1984), Fig. 1.

sets are available. It will be shown how the model, even in its extreme parsimony, can give qualitative and in some cases quantitative information on the spatial and temporal distributions of nutrients and phytoplankton in the Mediterranean Sea, together with a justification of the model's functioning in terms of biogeochemical energy availability.

In Section 2, a conceptual model description is firstly introduced and then the influence of the light limitation on the phytoplankton cycle in the Mediterranean is discussed. In light of these considerations, an analysis of the situations in different areas of the basin is considered. In Section 3 also some in situ data for comparison are shown. Then, in Section 4, surface chlorophyll maps, as obtained from the model results, are presented for elucidating the seasonality of the model near surface; analogous maps obtained from CZCS data are also shown. In Section 5 the findings obtained through this coupled model are discussed, both in case of water column and areal distribution.

## 2. The conceptual model

The three-dimensional model gives the space and time evolution of inorganic nitrogen $N$, phytoplankton $P$ and detritus $D$, all in nitrogen units. The aggregated equations are

$$\frac{\partial N}{\partial t} = -(\vec{u}\cdot\nabla)N - K_{\mathrm{H}}\nabla_{\mathrm{H}}^4 N + K_{\mathrm{V}}\frac{\partial^2 N}{\partial z^2} - FP + rD, \quad (1)$$

$$\frac{\partial P}{\partial t} = -(\vec{u}\cdot\nabla)P - K_{\mathrm{H}}\nabla_{\mathrm{H}}^4 P + K_{\mathrm{V}}\frac{\partial^2 P}{\partial z^2} + FP - dP, \quad (2)$$

$$\frac{\partial D}{\partial t} = -(\vec{u}\cdot\nabla)D - w_{\mathrm{D}}\frac{\partial D}{\partial z} - K_{\mathrm{H}}\nabla_{\mathrm{H}}^4 D + K_{\mathrm{V}}\frac{\partial^2 D}{\partial z^2} - rD + dP. \quad (3)$$

The limiting factor $F$ for the phytoplankton growth depends on the temperature, on the irradiance and on the Michaelis–Menten uptake; $d$ is the respiration and mortality rate for phytoplankton, while $r$ and $w_{\mathrm{D}}$ are respectively the detritus regeneration rate

Fig. 3. First, second and third year Hovmoller Diagram (run 14) for a sample station in the Ligurian Sea (44.25N 9E); DIN contoured, phytoplankton shaded above (both in mmol N $m^{-3}$); temperature contoured; salinity shaded beneath.

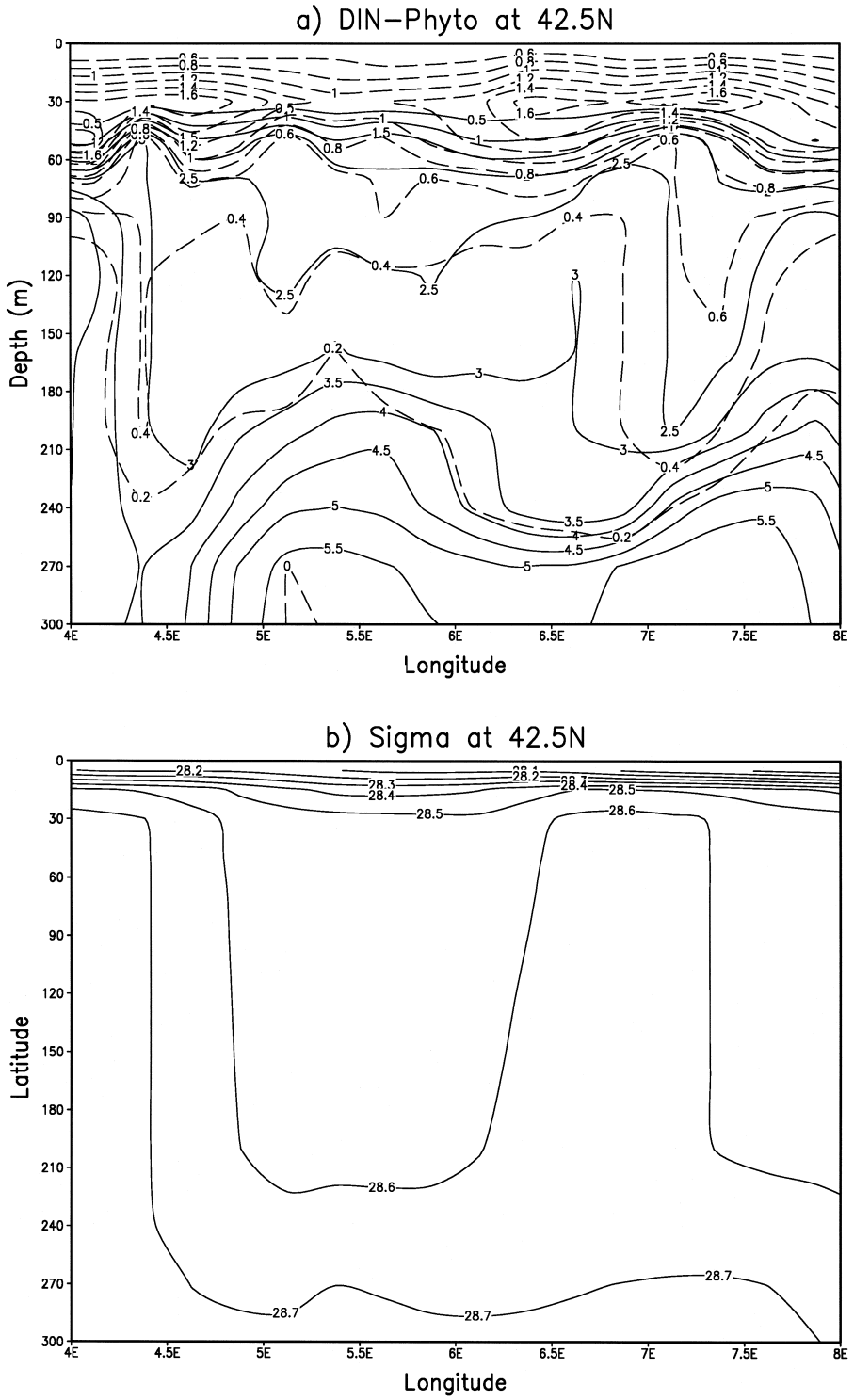


Fig. 5. (a) Second year transect (run 14) in Balearic Sea (42.5N 4–8E); DIN full line, phytoplankton dashed line (both in mmol N $m^{-3}$); (b) Sigma in the same transect as in (a).

and sinking velocity. The parameter values and the initial conditions are reported by Crise et al. (1998) (respectively, Table 1 and Figs. 2 and 3). An analysis of the equilibria of the reaction terms of the Eqs. (1)–(3) is given in Appendix A, taking into account also the potential influence of a zooplankton compartment.

The dead organic matter in all its forms plays a crucial role in maintaining the trophic equilibrium in the productive zone, balancing the inputs of inorganic nutrients on a global scale (Eppley and Peterson, 1979). The detritus state variable brings together three operational compartments: dissolved organic nitrogen, aggregates and fecal pellets. Different values of remineralization rates were tested by sensitivity analysis giving total yearly nitrogen fluxes at the Gibraltar and Sicily Straits (Crise et al., 1998; Table 3), in good agreement with those estimated from field data. The conclusion was that these parameterizations reasonably simulate the net effect of biological pumping in the basin, with a nitrogen total loss at Gibraltar evaluated in $2.36 \times 10^6$ tons/year during

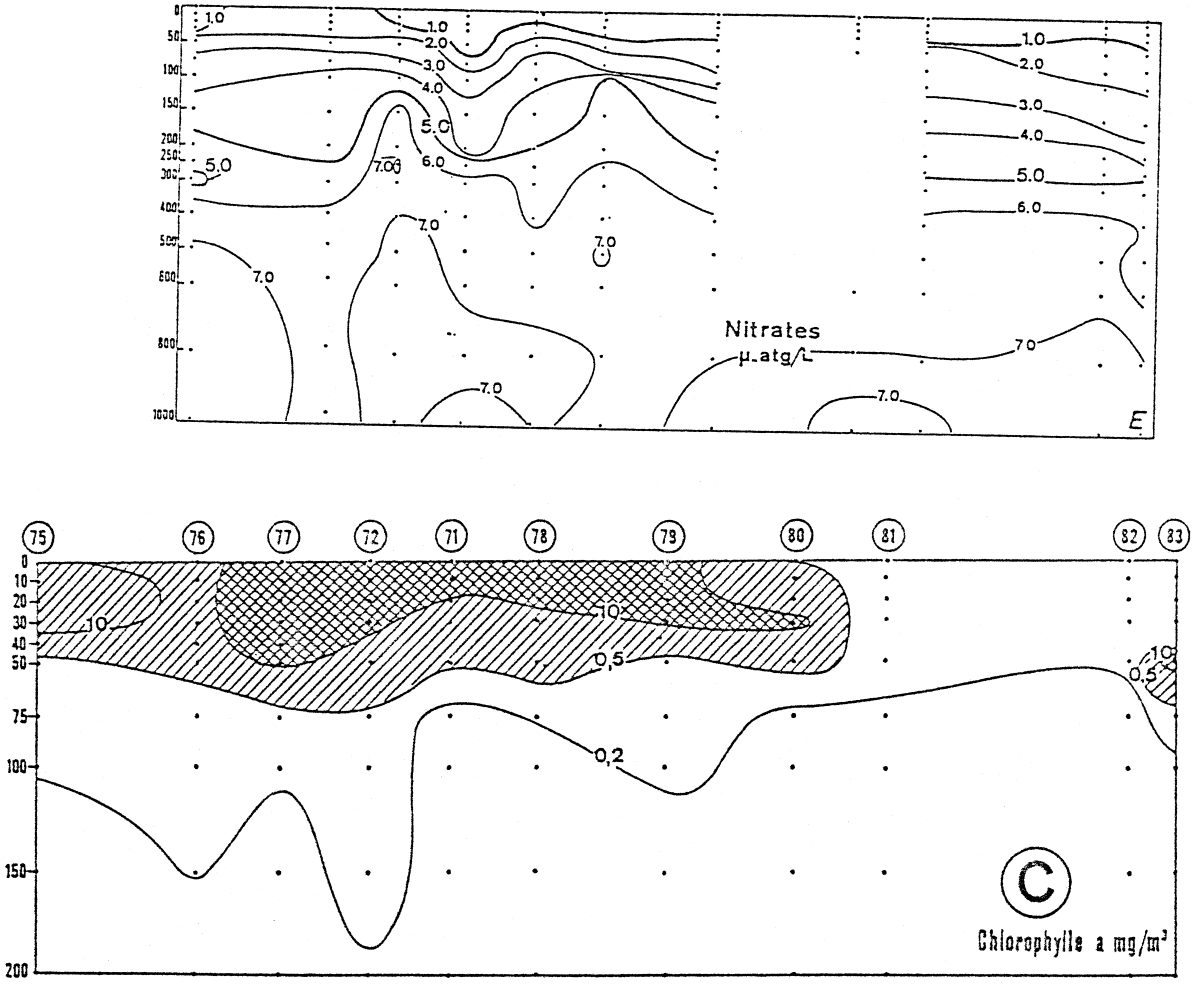


Fig. 6. Nitrate distribution (μatg/l) transect at 42.5N 4–8.5E above, after Coste et al. (1972), Fig. 22E; chlorophyll-*a* distribution (mg $m^{-3}$) in the same transect beneath, after Jacques et al. (1973), Fig. 2C. The left part of both plates coincides with (42.5N 4E) and the right ones with (42.5N 8.5E).

the second year of the b14 simulation, reported in this paper for an analysis of the results. Moreover the phytoplankton growth reaches a quasi-stationary cycle after about one year of simulation. The advantage of using such a simple aggregated description is twofold: firstly the results of this approach can be considered an overall information on the ecosystem components; secondly, by comparing these results with functional based ones, the generic ecosystem function is going to emerge.

The primary production in this trophic model is limited by the interplay between nitrogen available along the water column, determined by biomass uptake and by hydrological conditions, and the irradiance, expressed as a meridionally variant non-spectral formulation, and considering also the monthly

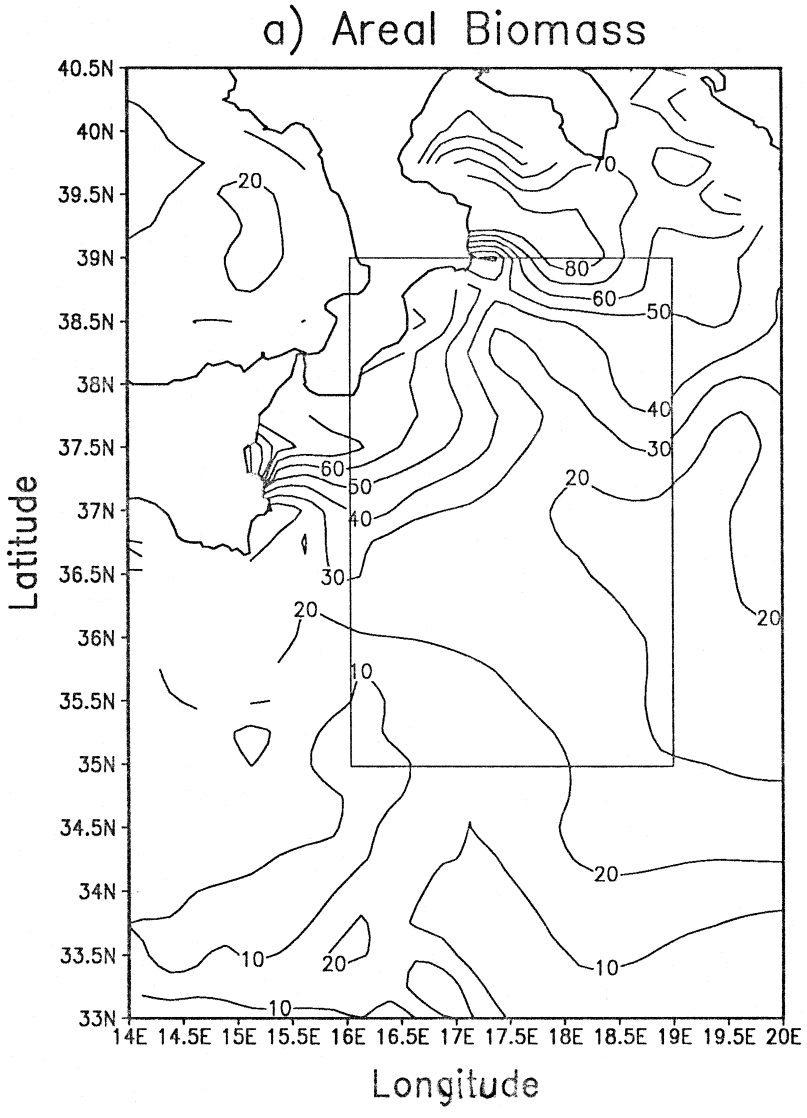


Fig. 7. (a) Second year areal biomass in October (run 14) in the Ionian Sea integrated in the surface layer down to 220 m (mmol N $m^{-2}$); (b) Second year vertical averaged phytoplankton in October (run 14) in the Ionian Sea 35–39N 16–19E box shown in Fig. 4a (mmol N $m^{-3}$).

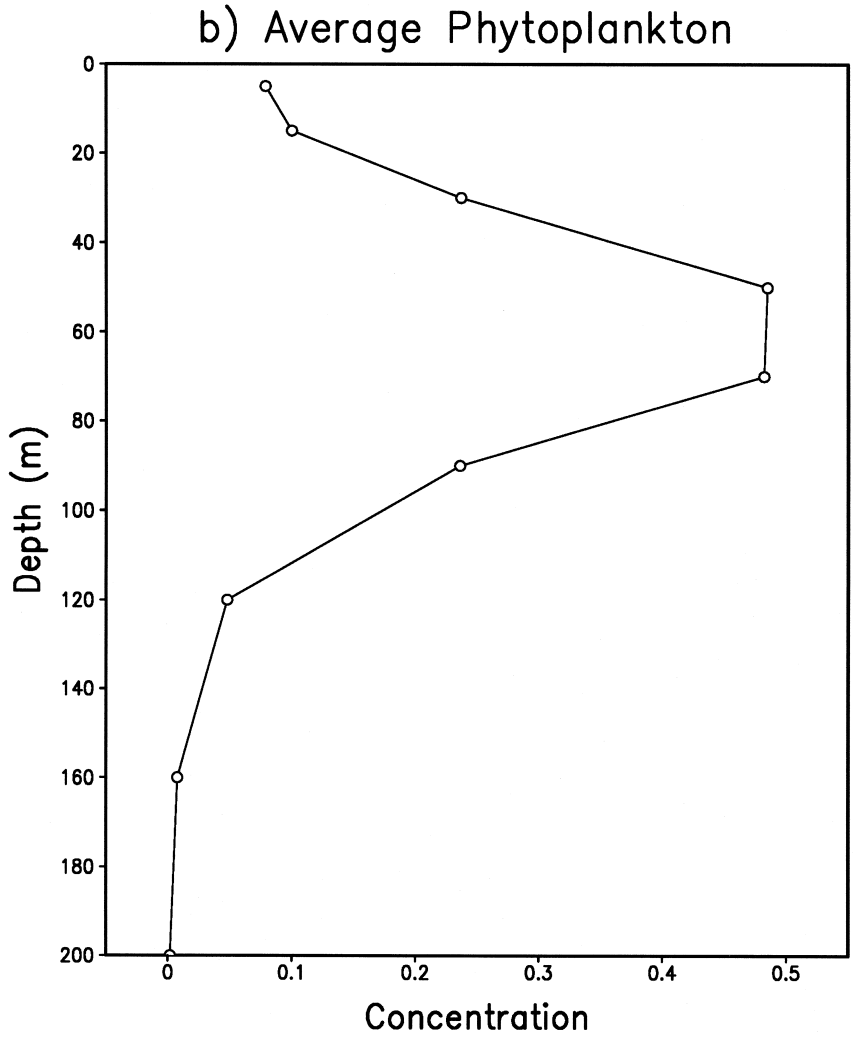


Fig. 7 (continued).

averaged cloud absorption. The feedback of biology on light penetration depth was turned off in the model, but a zonally variant light extinction coefficient was used, as reported in Fig. 1. This was obtained after interpolation from Secchi disk data measured during the POEM cruises for the eastern Mediterranean, and the EROS 2000 project for the western.

The transformation of the biomass data in chlorophyll concentrations, shown in the fifth section, is obtained using the following procedure. First an average of the concentration of the first 20 m is taken. This is a reasonable choice, because the optical length is about 15 m in the western Mediterranean and reaches approximately 30 m in the eastern. Then the C:N ratio of Redfield et al. (1963) is utilized to obtain the carbon equivalent of the calculated biomass expressed in nitrogen units. Finally the statistical model of Cloern et al. (1995) is applied to transform the carbon equivalent into chlorophyll-*a* concentrations with the following equation:

$$\mathrm{CHL} = 0.003 + 0.0154 e^{0.050T} e^{-0.0059I} \frac{N}{N + C_{\mathrm{N}}} \mathrm{CAR}. \quad (4)$$

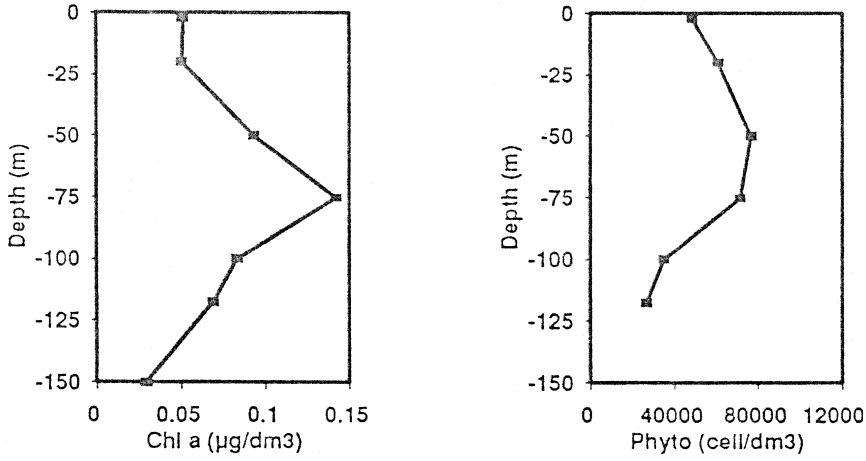


Fig. 8. Averaged vertical profiles of chlorophyll-*a* (μg $dm^{-3}$) left, phytoplankton (cell $dm^{-3}$) right in the Ionian Sea, after Rabitti et al. (1994), Fig. 4.

Here CHL is the chlorophyll concentration (mg Chl $m^{-3}$), $T$ is the temperature (°C), $I$ is the irradiance (mol quanta $m^{-2}$ $day^{-1}$), $N$ is the modelled inorganic nitrogen concentration (mg at. N $m^{-3}$), $C_N$ is the nitrate half-saturation (same units as $N$) and CAR is the phytoplankton concentration expressed in carbon (mg at. C $m^{-3}$). This formulation depends on the daily averaged irradiance, on the temperature and on nutrient availability. The chlorophyll is therefore diagnostically calculated assuming $I$ and $C_N$ as parametrized in the model. Such a transformation was performed on the surface biomass. The depth dependent analysis of open ocean phytoplankton requires a reassessment of the above statistical transformation of biomass into chlorophyll (as well as of the deterministic three-dimensional model) in terms both of the adaptive response of the different phytoplankton species present in the basin to the photosynthetic available radiation and of the effects of the turbulence conditions on the biomass growth.

## 3. Phytoplankton cycle

In the following some results of the model, analyzed consistently with experimental data acquired in different areas of the Mediterranean Sea, will be reported. Such areas are evidenced in Fig. 2.

The station sampled in the Ligurian Sea (Fig. 3) at 44.25N 9E exhibits a seasonal cycle with a phytoplankton maximum in May of about 1.2 mg at. N $m^{-3}$, while there is a decrease towards a minimum of activity in the months of November and December, reaching values lower than 0.2 mg at. N $m^{-3}$. The winter dynamics mix the water column down to 170 m, as evidenced by the Fig. 2b, while the deep bloom begins only in spring. The nutricline is remarkably stable because of a good balance between vertical mixing and convection of inorganic nitrogen, and the export of detrital matter from the euphotic zone.

In Fig. 4, after Fabiano et al. (1984), a temporal series of in situ chlorophyll measurements is shown. The trend is quite similar to the seasonal variation obtained from the model. The March samples of the chlorophyll-*a* exhibit homogeneous distribution throughout the water column to 170 m depth, while they indicate a maximum in April–May at 50 m. In summer the deep chlorophyll maximum (DCM) is present at 70 m and the model reproduces reasonably well the biomass maximum depth.

Fig. 9. Second year Hovmoller Diagram (run 14) at a sample station in the Levantine Basin (33N 34E); DIN contoured, phytoplankton shaded above (both in mmol N $m^{-3}$); temperature contoured, salinity shaded beneath.

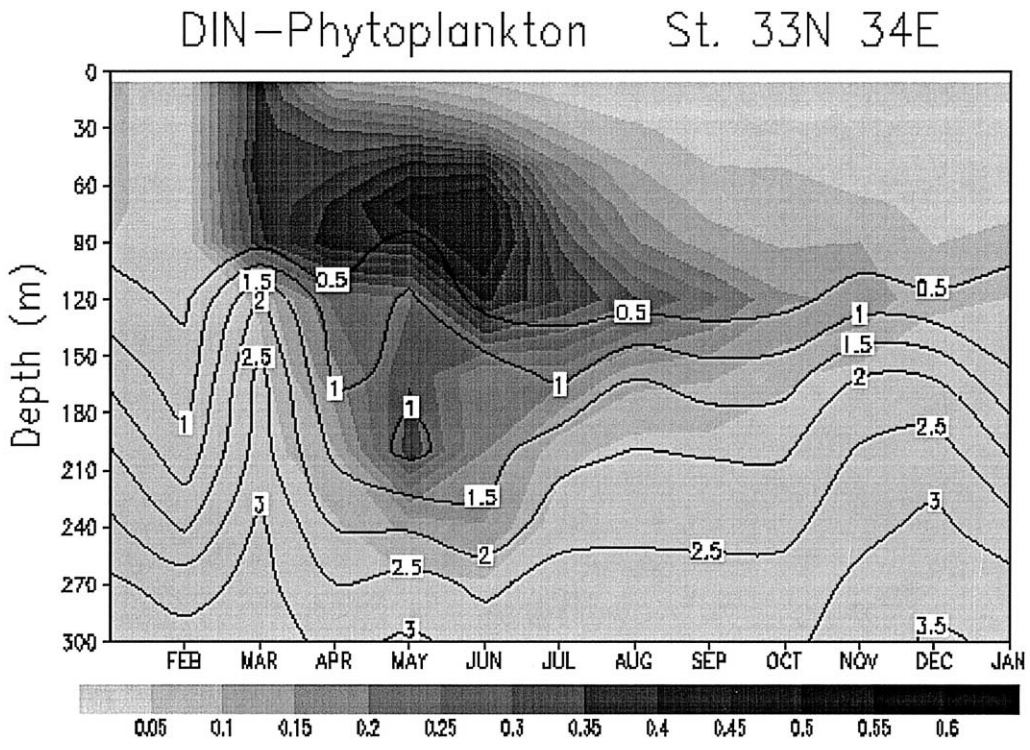
DIN–Phytoplankton St. 33N 34E
Depth (m)
0
30
60
90
120
150
180
210
240
270
300
FEB MAR APR MAY JUN JUL AUG SEP OCT NOV DEC JAN
0.05 0.1 0.15 0.2 0.25 0.3 0.35 0.4 0.45 0.5 0.55 0.6

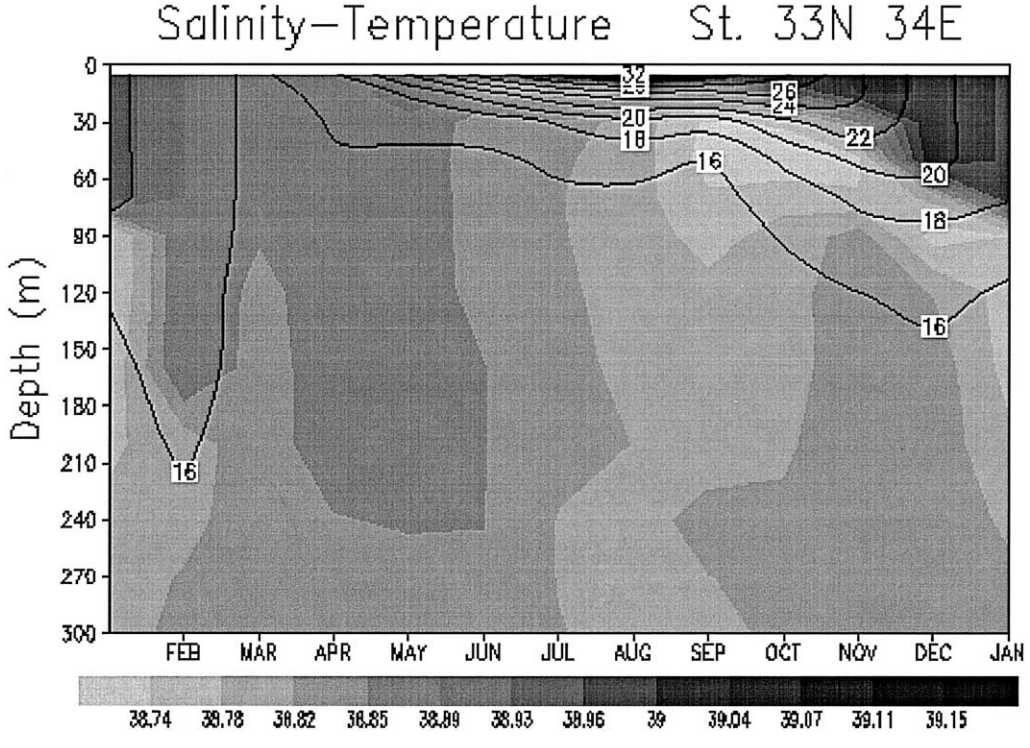
Salinity–Temperature St. 33N 34E
Depth (m)
0
30
60
90
120
150
180
210
240
270
300
FEB MAR APR MAY JUN JUL AUG SEP OCT NOV DEC JAN
38.74 38.78 38.82 38.85 38.89 38.93 38.96 39 39.04 39.07 39.11 39.15

In the Provençal Sea transect (42.5N 4–8E), the phytoplankton maximum (about 1.6 mg at. N $m^{-3}$) is recognizable in April (Fig. 5a) and is present at 30 m, but not homogeneously along the transect. The biomass still has a concentration greater than 0.2 mg at. N $m^{-3}$ down to 200 m depth, corresponding to residual winter mixing effects. The value for nitrogen concentration is about 2.0 mg at. N $m^{-3}$ at the light penetration depth (here about 60 m), with the inorganic nitrogen isolines nearly flat throughout the region under consideration. In the aphotic zone the situation is more dynamic. The confirmation that this is due essentially to the hydrodynamical conditions come from the potential density $\sigma$, plotted in Fig. 5b. Under 270 m we can see increasing $\sigma$ values at the same positions where inorganic nitrogen increases in depth. On the other hand, the upwellings of nitrogen, which generate the maxima of phytoplankton concentrations, correspond to $\sigma$ domings.

In Fig. 6a, an experimental transect acquired in April (Coste et al., 1972) shows that the nitrogen content at the base of the penetration depth is approximately 2.5 mg at. N $m^{-3}$. Beneath this quota we observe a downward shift of 50 m of the nitrogen in the data compared to the model, but nevertheless there is a good accord in the dome positions. We should stress here that this comparison is done only with the data taken in April in the second leg of the MEDIPROD I cruise, because winter data, collected in the first half of the cruise, were used for initializing the model with a homogeneous lateral profile. Biological data do not show a DCM, see Fig. 6b after Jacques et al. (1973). The model reproduces the western intensification in the chlorophyll-*a* present in the data and also shows a discontinuity between the subsurface peak located around 4E and the relative maximum present in the centre of the transect. The order of magnitude of the values obtained by the model after biomass to chlorophyll transformation, as shown in the next paragraph, are in good accord with the surface chlorophyll data.

In the Ionian Sea the depth integrated concentration of modelled phytoplankton, down to 220 m, is shown for October (Fig. 7a). The biomass near the Otranto sill and along the Calabria and Sicily coast is about three times that present at the centre of the basin. This is due to the relatively nutrient rich water exiting from the Adriatic Sea, and to the total effect of the upwelling. A meridional gradient in the integrated biomass is also evident, with higher values in the north and lower values in the south of the basin. The average vertical phytoplankton concentration, evaluated in the box drawn inside the Fig. 7a, is also shown in Fig. 7b. The maximum is here reached between 50 and 70 m, with a value of 0.5 mg at. N $m^{-3}$. This result confirms the disappearance below 100 m of the phytoplankton due to light limitation. This is in good accord with the fact that, in absence of lateral and vertical dynamics, there is a maximum, under which a biological quasi-stationary cycle is not possible. The maximum value here is about five times greater than that obtained at the surface, due to the balance between the light penetration depth, 92 m in the Ionian Sea, and the upwelling in the area.

These structures captured in the model are recognized in the October data, collected by Rabitti et al. (1994) during POEM-BC-O91 (Fig. 8). The model reproduces well the deep biomass maximum (Fig. 8b), measured during that cruise, while the maximum surface ratio exhibited by the simulation is nearer to the chlorophyll experimental profile (Fig. 8a) than that of the phytoplankton.

The behaviour of a water column time evolution (Hovmoller diagram) in the Levantine basin at 33N 34E shows the dynamics of the inorganic nitrogen and phytoplankton concentrations during the second year simulation (Fig. 9). The temperature and salinity diagrams are also shown. The maximum of phytoplankton is here obtained at 90 m (biomass about 0.6 mg at. N $m^{-3}$) during May and June. After this bloom period the subsurface maximum deepens to about 120 m, which is the light extinction depth in this area.

In the Levantine Sea, a comparison is possible with the available chlorophyll profiles from different sites within the sub-basin in different seasons, as shown in Fig. 10, after Berman et al. (1986). The effect of the decreased light extinction coefficient is evident, and the DCM sampled in situ is at a similar depth to the biomass maximum given by the model. The trend of seasonal variations is approximately the same: there is a maximum in May–June as in measurements, and the increase in depth of chlorophyll-*a* data is reproduced by the model.

Some quantitative comparisons are attempted in Section 4 considering chlorophyll data recorded at

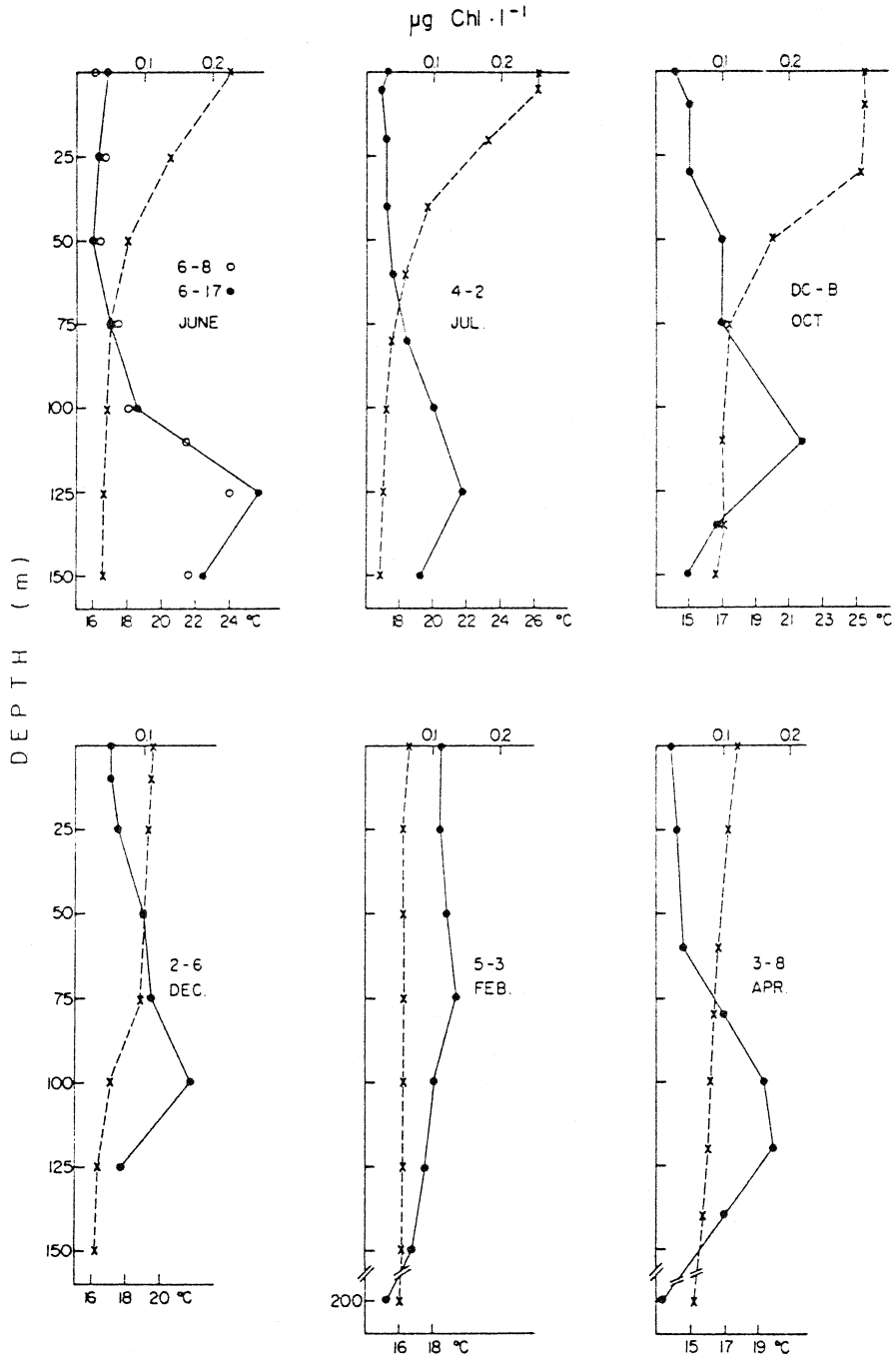


Fig. 10. Depth profiles of chlorophyll (∘----∘) in µg $l^{-1}$ and temperature (x————x) in °C at Levantine basin stations in different seasons, after Berman et al. (1986), Fig. 5.

the surface either by means of in situ data or considering postprocessed satellites images.

For a depth-dependent comparison of the biomass signal, we take here into account the depth of the

Table 1
Observed depth (m) of the DCM

| Area | Winter | Spring | Summer | Autumn | Reference |
|---|---|---|---|---|---|
| Alboran Sea (Modified Atlantic water) | | 30/36 | | | Lohrenz et al., 1988 |
| Alboran Sea (Mediterranean-type water) | | 60/64 | | | Lohrenz et al., 1988 |
| Alboran Sea | | 20/30 | | | Delgado, 1990 |
| Alboran Sea (1°–2°W) | | | | 54 | Gould and Wiesenburg, 1990 |
| Alboran Sea (Almeria–Oran front) | | 30 | | | Arnone et al., 1990 |
| Alboran Sea (Algerian current 1°E) | | 25/65 | | | Arnone et al., 1990 |
| Alboran Sea (Algerian current 3°E) | | 35/75 | | | Arnone et al., 1990 |
| Catalan Sea | | | | 50/100 | Estrada, 1981 |
| Catalan Sea | mixed | 40/50 | | | Delgado et al., 1992 |
| Catalan–Balearic region | 80/90 | 70/80 | 85/95 | | Estrada et al., 1993 |
| Balearic Sea (southern region) | | | 65/80 | | Berland et al., 1988 |
| Ligurian Sea | | | 40/60 | | Jacques et al., 1976 |
| Ligurian Sea (divergence zone) | | | 50 | | Jacques et al., 1976 |
| Ionian Sea | | | 75/95 | | Berland et al., 1988 |
| Cretan Sea | | | 75/95 | | Berland et al., 1988 |
| Levantine Basin | | | 90/120 | | Berland et al., 1988 |
| Levantine Basin (southern region) | | 100 | 100/125 | 75/100 | Kimor et al., 1987 |
| Levantine Basin (Cyprus eddy core) | mixed | 100 | 110 | 80 | Krom et al., 1993 |
| Levantine Basin (Cyprus eddy boundary) | mixed | 100 | 90 | 80 | Krom et al., 1993 |

DCM as measured in the Mediterranean Sea (Table 1). All the regions considered by the reported authors are open sea areas; elsewhere they considered for the analysis only stations beyond the continental shelf. For the Catalan–Balearic region all the frontal area is taken into consideration, and this can explain the high range of variation in that region, anyway in keeping with the overall trend. In this area the winter mixing determines nearly homogeneous chlorophyll concentrations in the upper 70 m layer; in the Cyprus eddy the mixing in the same season covers about 120 m (125 m inside the core).

These data cover a large area of the Mediterranean basin in terms of open sea chlorophyll response and in term of time evolution, even not all the stations cover all the seasonal variability. In the course of the same cruise and in the same area, the DCM vary considerably from station to station. After a prevalent mixed winter situation the DCM deepens from spring to summer, reaching a nearly stable situation, but subject to the new mixing beginning in late autumn. This behaviour is evident in the evolution of the model, for example, Fig. 3, with a maximum present till the end of October. Thirdly increasing depths of DCM are recovered from west to east, from 30/40 m in the Alboran Sea to 100/125 m in the Levantine basin. Also this pattern is recognizable in the model comparing Figs. 3 and 9.

## 4. Surface chlorophyll

The result for the chlorophyll concentration in the first 20 m is shown in Fig. 11 for the second year simulation, where a constant offset of 0.04 mg Chl $m^{-3}$ is added.

For January (Fig. 11a) the first layer bloom is evident in the modelled chlorophyll, in particular in the western Mediterranean. This is due to the deep nitrogen contributions to the winter mixing. The meandering of the Modified Atlantic Water is evident, and its flow along the African coast due to the prevalent westerly wind regime in the Ionian Sea.

In April (Fig. 11b) a clear west–east gradient is evident, with a maximum in the Alboran Sea and in the Ligurian–Provençal basin, and a minimum in the Levantine Sea. In particular, the Alboran Sea lower production due to the anticyclonic circulation is evident, as well as the Spanish coast upwelling in the

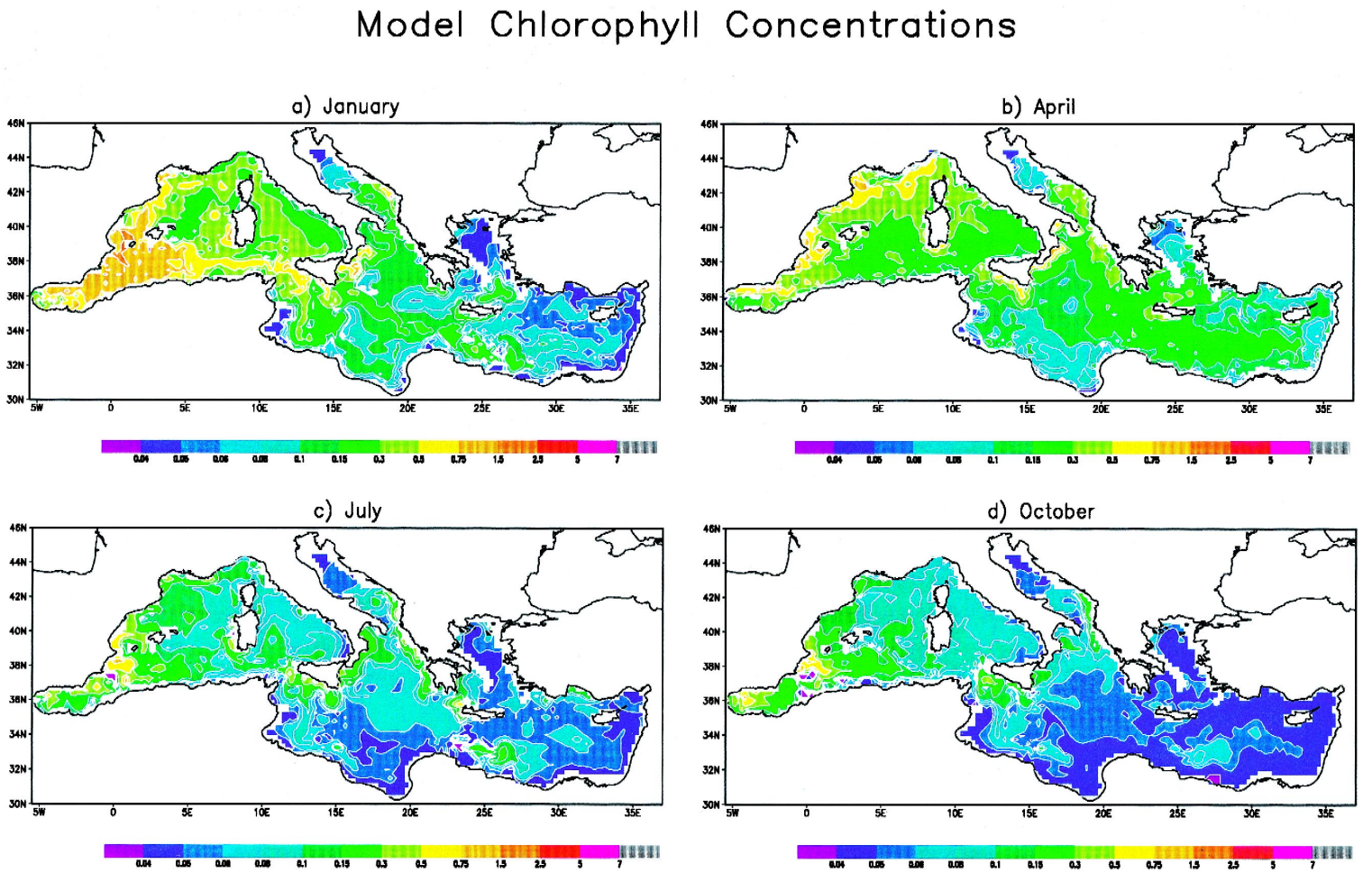


Fig. 11. Chlorophyll surface concentration in (a) January, (b) April, (c) July and (d) October obtained from the NPD model (see formula 4) for the first 20 m (mg Chl $m^{-3}$).

Balearic Sea. In the Ligurian–Provençal basin the strong effect of convection determines a well localized increase in biomass. Also evident are the biological effects caused by upwelling along the south coast of Sardinia, Sicily and the south–east coast of Italy. The north–south gradient in the Ionian Sea, with higher values in the north and lower ones in the Sirte Gulf, is also clearly seen.

In July (Fig. 11c) the summer depleted situation is almost reached and the influence of the Atlantic Water is now more active in the eastern basin, where the zonal distribution due to the circulation tends to stabilize.

In October (Fig. 11d) the model chlorophyll concentration is depleted and follows the circulation patterns, with minima in the southern regions and in the Levantine basin, and maxima in the Alboran Sea and in the Balearic Sea. The Sicily coast is still affected by the upwelling effects.

An overall picture can be extracted from this sequence of images. For the seasonal cycle we see that the maxima are obtained in January, with a subsequent diminution of surface chlorophyll concentration. In summer the pigment concentration shows its lowest values, while in October we see an increase in pigment concentrations, particularly where upwelling or eddies are present. Generally the patterns are lower in the eastern part than in the western, where there is also a greater seasonal variability.

For comparison we consider the level 3 monthly mean CZCS data obtained by the Nimbus-7 satellite from 1978 to 1986, as analyzed at the Goddard Space Flight Center. The chlorophyll is obtained, after climatological averaging, from the raw data, RD, using the formula

$$\mathrm{CHL} = 10^{0.012\,\mathrm{RD} - 1.4} \qquad (5)$$

One should note that the CZCS data include not only chlorophyll, but also all the other pheopigments.

The values obtained by the model are in good agreement with the winter data (Fig. 12a), more so in the western part of the basin than in the southern. A strong under-estimation of chlorophyll in the Adriatic and Aegean Seas is also evident. This could be due to two principal reasons: the Po and Bosphorus inflows of nutrient rich water are completely disregarded in the model, and the benthic–pelagic coupling is not included in the description of these shallow marginal seas. The influence of all these approximations does not seem, at least for the three years spanned by the simulation, important to the open ocean response. However, the maxima obtained by the model, 2.5 mg Chl $m^{-3}$, are of the same order as the satellite data, even if these highest values are found in an area larger in data than in model.

Also for April (Fig. 12b) the numerical values fit the general distribution of CZCS averages for the same period in the western part of the basin, reaching a maximum of about 1.5 mg Chl $m^{-3}$, while for the eastern part, greater values are obtained in the model than in CZCS data. In particular the Sicily and Sardinia upwellings seem to be overestimated in the model.

The summer situations discussed above are, broadly speaking, confirmed by the situation in July (Fig. 12c). The model results seem to be affected more than the data by the sub-basin dynamics, but the main features of the oligotrophy in the eastern Levantine basin are well captured, with values less than 0.05 mg Chl $m^{-3}$.

The comparison with CZCS data in October (Fig. 12d) is good in qualitative terms, always giving a clear west–east gradient and pronounced zonal structures, but the values, in particular in the eastern basin, are significantly lower than the data. This could be due to the CZCS overestimation of chlorophyll content, due to the processed signal comprising not only biomass, but also dead matter.

As a final comment, there is a significant correspondence both in temporal evolution and in spatial distribution between the CZCS data and the model results for the open ocean. The west–east gradient is evident, and the north–south gradients from the Ligurian to the Balearic Sea and in the Ionian Sea are well defined, in particular in the late winter situation.

The values of very low surface chlorophyll concentrations in the eastern Mediterranean almost throughout the year fit pretty well with model predictions and CZCS images, while higher values in the western Mediterranean are given by both model and remotely sensed results. These differences can be explained by the fact that the remote sensing algorithms calibrated for the open ocean do not work properly in coastal waters, where higher chlorophyll

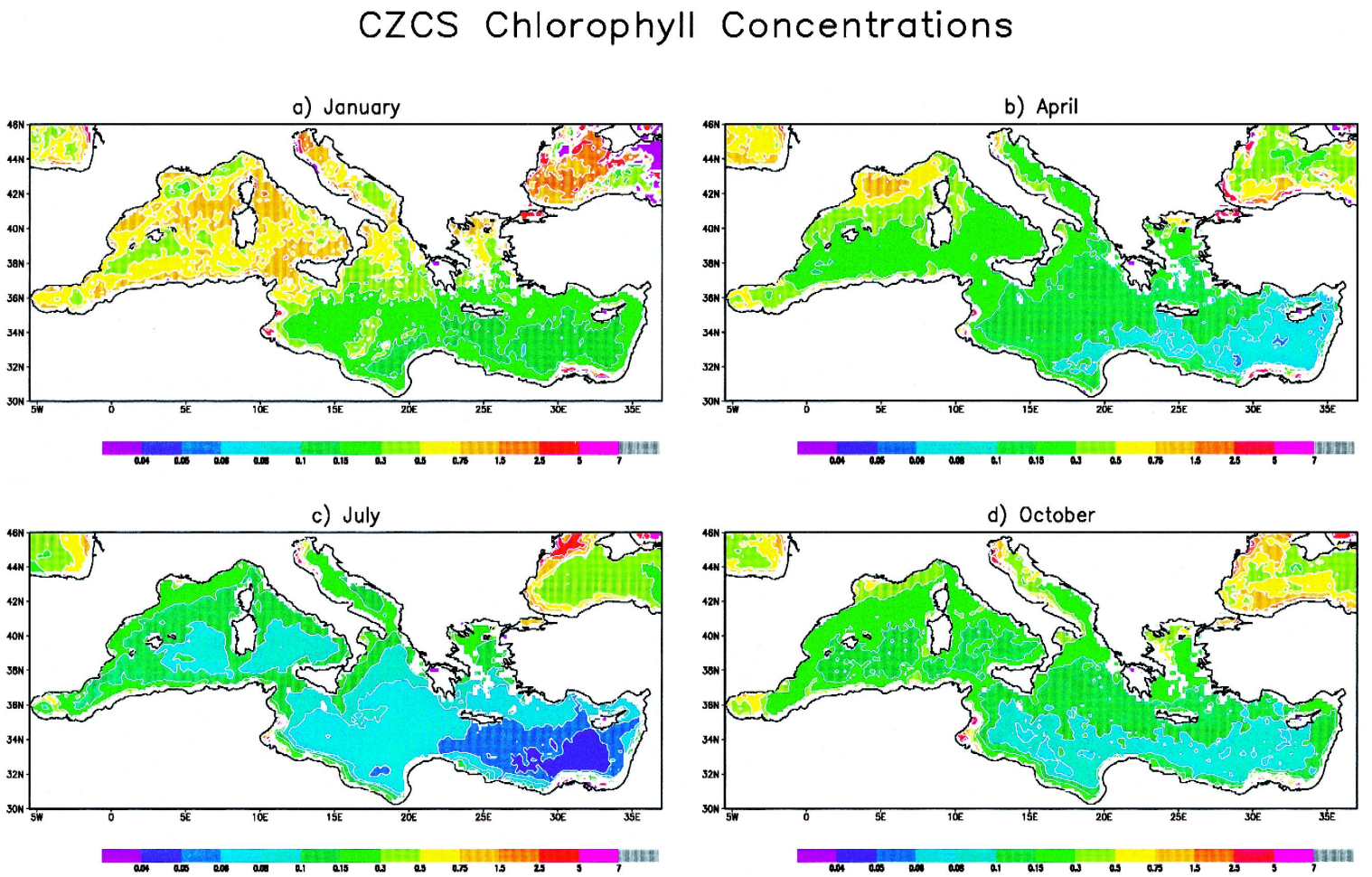


Fig. 12. Chlorophyll surface concentration in (a) January, (b) April, (c) July and (d) October obtained from the CZCS data for the years 1978–1986 (mg Chl $m^{-3}$).

Table 2
Observed surface chlorophyll concentrations (mg Chl $m^{-3}$)

| Area | Winter | Spring | Summer | Autumn | Reference |
|---|---|---|---|---|---|
| Alboran Sea (1°–2°W) | | | | 0.6 | Gould and Wiesenburg, 1990 |
| Alboran Sea (Almeria–Oran front) | | 0.2/1.5 | | | Arnone et al., 1990 |
| Alboran Sea (Algerian current 1°E) | | 0.1/0.2 | | | Arnone et al., 1990 |
| Alboran Sea (Algerian current 3°E) | | 0.1/0.2 | | | Arnone et al., 1990 |
| Alboran Sea | | | | 0.3/3 | Minas et al., 1991 |
| Balearic Sea (southern region) | | | 0.13 | | Berland et al., 1988 |
| Ligurian–Provençal Sea (frontal zone) | | 0.14/0.46 | | | Berland et al., 1973 |
| Ligurian–Provençal Sea (intermediate zone) | | 0.4 | | | Berland et al., 1973 |
| Ligurian–Provençal Sea (periferic zone) | | 0.35 | | | Berland et al., 1973 |
| Ionian Sea | | | 0.09 | | Berland et al., 1988 |
| Ionian Sea | | | | 0.05 | Rabitti et al., 1994 |
| Cretan Sea | | | 0.09 | | Berland et al., 1988 |
| Levantine Basin (Israeli pelagic station) | 0.22 | 0.07 | 0.12 | 0.15 | Azov, 1986 |
| Levantine Basin (southern region) | 0.12 | 0.03/0.04 | 0.03 | 0.07 | Berman et al., 1986 |
| Levantine Basin | | | 0.09 | | Berland et al., 1988 |

concentration as well other optically-equivalent suspended matter is found. Some of the measurements exclude the picoplankton contribution that could be significant, at least in some seasons.

For a more complete discussion we report in Table 2 different ship measurements of the surface layer chlorophyll in different areas of the Mediterranean Sea. The reported values are taken from sampled stations considered by the authors, and the variability range inside the same cruise is due to the influence of the specific small scale processes. For the Israeli coast pelagic station an average on the original seasonal values was performed.

In the Alboran Sea the model results are in good accord with the spring and autumn data, also considering the high variability recorded in this area by Minas et al. (1991). In the Ligurian Sea the model results overestimate respect to the spring data. In some sense the model results in this area lie between the measured data and the satellite outcomes. In the Ionian Sea the model confirms a decreasing of the surface chlorophyll during summer to autumn transition. In the Levantine basin the model reproduces values generally lower than data, taking also into account their strong variation.

Thus the in situ evidences collected in Table 2 show the same spatial pattern, even if the seasonality is not always clear and care must be taken in pooling together measurements made with different techniques.

## 5. Discussion

The water column evolution plots presented in this work exhibit both similarities (energetic late winter mixing followed by stratification, formation and permanence of a DCM for most of the year) and striking differences (nutrient availability, nutricline and deep biomass maxima depths, different start times for the spring–summer stratification regime) which are supported also by experimental results. Conversely, the trophic part of the model is not space-variant, with the important exception of the light extinction coefficient which is derived from experimental measurements. Moreover, the biogeochemical initial conditions are laterally homogeneous profiles for phytoplankton and detritus, while the nutrients are initialized with an areal stepwise nitrate function. These highly idealized initial conditions for the biogenic component evolve in the upper layer into a space-dependent distribution which has a significant seasonally variant trophic response. This means that the influence of the physical forcings, as simulated by this coupled three-dimensional model,

affects not only the seasonal response but is able to induce large modifications to the seasonal cycles on a regional base.

To properly simulate the details of phytoplankton dynamics in the Mediterranean Sea would require a much more detailed food web modelling to assess the complex relationships between the nutrient driven trophic cycles and the microbial loop (Evans and Fasham, 1993). Nevertheless, the influence of the limiting factors on the autotrophic production reproduced by the model seems to be accurate enough to schematically reproduce an *ecosystem energy conditioning*, as comparison with the observations seems to support.

This aggregated formulation suggests that the onset and evolution of the deep biomass maximum can be explained only in terms of physical processes, following basically a stratigraphic approach (Kiefer and Kremer, 1981; Varela et al., 1994). Even though phytoplankton sinking rates are often prescribed (Steele and Yentsch, 1960; Jamart et al., 1977) the present formulation is adapted to a phytoplankton fraction distribution where small fractions prevail, and where the vertical export of living and dead matter is negligible (Ducklow et al., 1986; Heussner and Monaco, 1995).

The common features found in the above discussed numerical examples show a winter 'reset' of the trophic conditions due to mixing and convection (earlier in the western Mediterranean). In this phase, the nutrient pool is established, which then gives way to a primary production increment. (With smooth forcings it is impossible to obtain realistic phytoplankton blooms.) At the beginning, primary production is faster above the pycnocline where light, nutrients and temperature sustain a momentary increase of biomass. This increment creates a nutrient scarcity more rapidly than in depth, because the export of biogenic material not remineralized within the upper layer progressively depletes the euphotic zone. Only later is the layer below the pycnocline progressively included in the productive layer. New production can thus be obtained by light penetration seasonal variability and not by vertical advection. At these depths, light limits the growth rate, preventing fast consumption of nutrients and maintaining the biomass in depth for a longer time. The detrital fall-out contributes to the nutrient refilling of this layer, recreating the conditions for another winter mixing, thus initiating again the seasonal cycle.

A much more impressive picture of the influence of the general circulation on phytoplankton spatial distribution is given by the surface phytoplankton distributions. In this case, a transformation from biomass to chlorophyll was attempted, exploiting the fact that the formula we used was calculated from tank measurements where no photoadaptation at low irradiance intensity was taken into account. The formula is suitable for converting the surface phytoplankton biomass for most of the year, even though it was calculated under eutrophic conditions. To fit the nutrient dependency of the Eq. (4) with the oligotrophy of the Mediterranean Sea, we resorted to modify the half-saturation constant that appears in Eq. (4) as in the Eqs. (1)–(3).

Some issues of the seasonal cycle can be explained in terms of the influence of the physical forcings on ecosystem dynamics: (1) the seasonal response presents large differences depending on geographical position; (2) the deep biomass maximum exhibits a pronounced tilt, shallower in the Alboran Sea and deeper in the Levantine Sea, with greater productivity in western than in eastern Mediterranean; (3) the cloud coverage shows its effect by increasing the dynamics of the seasonal cycle, depressing the primary production during winter and postponing the maximum productivity period.

The striking difference between the East and West Mediterranean is evident, considering the approximately double chlorophyll concentration in the latter with respect to the former in summer, while in winter this difference grows to an order of magnitude.

All the hydrodynamical processes characterizing the eastern sub-basin can induce directly or indirectly an oligotrophic regime: the absence of convective mixing due to deep water formation, the reduced influence of the wind driven coastal upwellings and the exchanges with marginal seas all seem to be favourable to a reduced import of nutrients. In particular this is true during the winter situation, which is known to be the period in which an accumulation of nutrients occurs in the productive zone.

The nutricline erosion by primary producers is stronger at depth, creating a deep nutrient-depleted layer where only regenerated production is present

and turbulent entrainment is difficult not only during summer, when stratification decouples the mixed layer from the biomass maximum, but also in winter. For this reason, the anticipation of the western Mediterranean winter bloom could be mainly connected to the shallower nutricline and energetic wind forcings that allow an ubiquitous increase of chlorophyll concentration even in the surface layer. In contrast, the eastern Mediterranean in January still has a deep nutricline, which is only affected when convection take place, typically later, at the end of winter.

In conclusion, the model was verificated against in situ and satellite data: basically it is able to resolve the main characteristics of the seasonal cycles, but also the time and space patterns of the bloom accord with the known phenomenology, and the order of magnitude of the obtained maxima is in keeping with the real data.

The model simulations also lead to an interpretation, based on coupled physical–biochemical processes, of the Mediterranean Sea trophic gradients and suggest a possible explanation for the different oligotrophic regimes and ecosystem response in the Mediterranean sub-basin.

**Acknowledgements**

The authors are indebted to Valentina Mosetti for managing the CZCS data. This work was partially funded by the EC contracts Mediterranean Eddy Resolving Modelling And InterDisciplinary Studies-II (MAS2-CT93-0055) and MAss Transfer and Ecosystem Response (MAS3-CT96-0051). All the figures were obtained with the public domain package GrADS.

## Appendix A

To capture some essential properties of the evolution of the proposed model in the Mediterranean Sea, in this Appendix an NPZD model will be considered. This model has four state variables: inorganic nitrogen, phytoplankton, detritus, and the zooplankton variable, to introduce a biomass-dependent grazing in the model. The equation system we want to discuss are:

$$\frac{\mathrm{d}N}{\mathrm{d}t} = -\frac{G_{\mathrm{TI}}N}{C_{\mathrm{N}}+N}P + rD + (1-\alpha)\,\delta Z \tag{6}$$

$$\frac{\mathrm{d}P}{\mathrm{d}t} = \frac{G_{\mathrm{TI}}N}{C_{\mathrm{N}}+N}P - dP - \gamma PZ \tag{7}$$

$$\frac{\mathrm{d}Z}{\mathrm{d}t} = \gamma PZ - \delta Z \tag{8}$$

$$\frac{\mathrm{d}D}{\mathrm{d}t} = dP + \alpha\delta Z - rD \tag{9}$$

These equations are exactly the same used in the present paper, with the introduction of a multiplicative zooplankton grazing and without the advection–diffusion–convection terms. The persistence of the zooplankton can be evidenced studying the equilibria of such a system.

The lowest equilibrium is obtained when the living matter is not present, i.e., $P = Z = D = 0$. For this case the balance requires

$$N = N_0 = \frac{dC_{\mathrm{N}}}{G_{\mathrm{TI}} - d} \tag{10}$$

where $N_0 = N + P + Z + D$ is the total nitrogen present in the closed system. This is the same condition that limits the phytoplankton persistence in the NPD formulation.

The intermediate equilibrium is attained when the zooplankton is still absent, but phytoplankton persistence is assured under the following conditions:

$$N = \frac{dC_{\mathrm{N}}}{G_{\mathrm{TI}} - d} \tag{11}$$

$$P = \left(N_0 - \frac{dC_{\mathrm{N}}}{G_{\mathrm{TI}} - d}\right) \Big/ \left(1 + \frac{d}{r}\right) \tag{12}$$

$$D = \frac{dP}{r} \tag{13}$$

The highest equilibrium is reached when all four variables persist and their values are

$$P = \frac{\delta}{\gamma} \tag{14}$$

$$Z = \frac{1}{\gamma}\left(\frac{G_{\mathrm{TI}}N}{C_{\mathrm{N}}+N} - d\right) \tag{15}$$

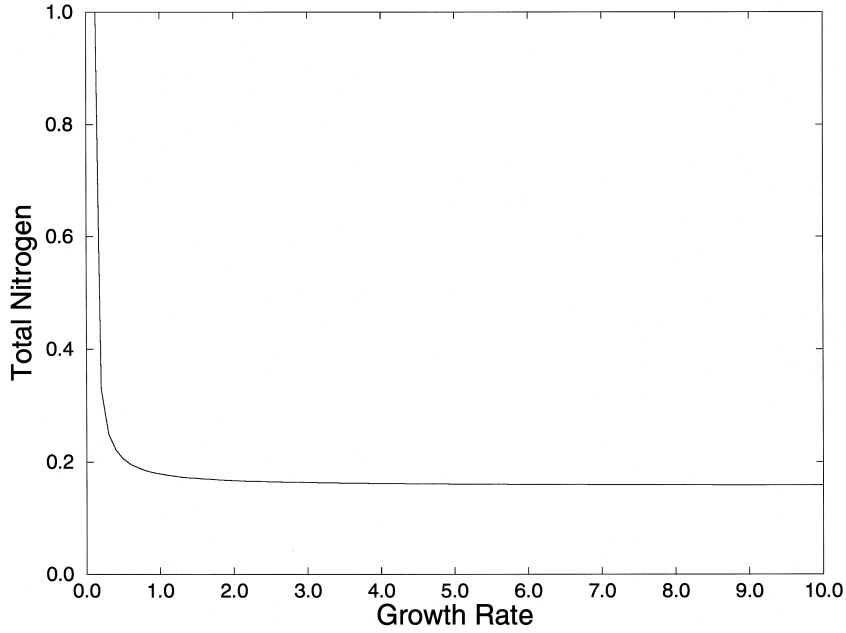


Fig. 13. Minimum total nitrogen (mg at. N $m^{-3}$) vs. growth rate (in units of maximum growth rate $G_{MAX} = 6.83 \times 10^{-6}$) at which zooplankton can persist.

$$D = \frac{G_{TI}\delta}{r\gamma}\frac{N}{C_N + N} + (1-\alpha)\frac{d\delta}{\tau\gamma} \tag{16}$$

The equilibrium for $N$ is the solution of the following quadratic equation:

$$r\gamma N^2 + AN - r\gamma C_N N_0 + (r\delta - rd + (1-\alpha)d\delta)C_N = 0 \tag{17}$$

with

$$A = r\gamma(C_N - N_0) + (\alpha\delta + r)G_{TI} + r\delta - rd + (1-\alpha)d\delta.$$

The persistence condition of the zooplankton (Fig. 13) emerges from the total nitrogen curve limiting the lowest, $Z = 0$, area from the highest, $Z \neq 0$, area. The parameters used are the same as in the three-dimensional model with $G_{TI}$ product of light and temperature factors, while for the zooplankton the parameters are, according to Fasham et al. (1990): $\gamma = 1.157 \times 10^{-5}$ $m^3$ (mg at. N)$^{-1}$ $s^{-1}$, $\delta = 1.736 \times 10^{-6}$ $s^{-1}$ and $\alpha = 1/3$. Two things can be appraised studying the asymptotes of this solution. The first one is that for large $G_{TI}$, $N_0$ is equal to

$$N_0 = \frac{1}{\gamma}\left(\delta - d + (1-\alpha)\delta\frac{d}{r}\right) \tag{18}$$

which for our parameter values is 0.150. This gives a clear correspondance between the calibration of the ecological system, in particular of the grazing and mortality rate for the zooplankton compartment, and its presence in all the stages of model evolution. The second asymptote, attained when $N_0$ goes to infinity, is $G_{TI} = d$, which is approximately one tenth of our $G_{MAX}$ parameter. When this value is reached, for example in waters with a low total effect of irradiance, the non-persistence of the total NPZD model, in favour of an NPD model, is obtained.

## References

Alarçon, M., Cruzado, A., 1989. Atmospheric dry deposition of nutrients at a Catalan coastal site of North Western Mediterranean. Proc. XXII Reunion Bienal de la Real Societad Española de Fisica. Univ. Iles Balears.

Aleem, A.A., Dowidar, N., 1967. Phytoplankton production in relation with nutrients along the Egiptyan Mediterranean coast. Proc. Int. Conf. Trop. Oceanography, pp. 305–327.

Arnone, R.A., Wiesenburg, D.A., Saunders, K.D., 1990. The origin and characteristics of the Algerian Current. J. Geophys. Res. 95 (C2), 1587–1598.

Azov, Y., 1986. Seasonal patterns of phytoplankton productivity and abundance in nearshore oligotrophic waters of the Levant basin (Mediterranean). J. Plankton Res. 8 (1), 41–53.

Berland, B., Bonin, D., Coste, B., Maestrini, S., Minas, H.J., 1973. Influence des conditions hivernales sur les productions phyto- et zooplanctoniques en Méditerranée Nord-Occidentale: III. Caractérisation des eaux de surface au moyen de cultures d'algues. Mar. Biol. 23, 267–274.

Berland, B.R., Benzhitski, A.G., Burlakova, Z.P., Georgieva, L.V., Izmestieva, M.A., Khodolov, V.I., Maestrini, S.Y., 1988. Condition hydrologiques estivales en Méditerranée, répartition du phytoplankton et la matière organique. Oceanol. Acta 9, 163–177.

Berman, T., Azov, Y., Schneller, A., Walline, P., Townsend, D.W., 1986. Extent, transparency, and phytoplankton distribution of the neritic waters overlying the Israeli coastal shelf. Oceanol. Acta 9, 439–447.

Béthoux, J.P., Copin-Montegut, G., 1986. Biological fixation of atmospheric nitrogen in the Mediterranean Sea. Limnol. Oceanogr. 31, 1353–1358.

Canals, M., Lipiatou, E. (Eds.), 1994. First Workshop of the Mediterranean Targeted Project—Extended Abstracts. Tesys-Barcelona, 285 pp.

Carrada, G.C., Hopkins, T.S., Bonaduce, G., Ianora, A., Marino, D., Modigh, M., Ribera D'Alcalà, M., Scotto di Carlo, B., 1980. Variabily in the hydrographic and biological features of the Gulf of Naples. Mar. Ecol. 1, 105–120.

Civitarese, G., Bregant, D., Luchetta, A., Rabitti, S., De Lazzari, A., Boldrin, A., Manca, B., Scarazzato, P., Souvermetzoglou, E., Krassakopoulou, E., 1995. Biogeochemical exchanges in the Strait of Otranto. In: Tzelepides, A., Wassman, P. (Eds.), Second Workshop on Mediterranean Targeted Project, p. 189.

Cloern, J.E., Grenz, C., Vidergas-Lucas, L., 1995. An empirical model of the phytoplankton chlorophyll:carbon ratio—the conversion factor between productivity and growth rate. Limnol. Oceanogr. 40 (7), 1313–1321.

Coste, B., Gostan, J., Minas, H.J., 1972. Influence des conditions hivernales sur les productions phyto- et zooplanctoniques en Méditerranée Nord-Occidentale: I. Structures hydrologiques et distribution des sels nutritifs. Mar. Biol. 16, 320–348.

Coste, B., Le Corre, P., Minas, H.J., 1988. Re-evaluation of the nutrient exchanges in the Strait of Gibraltar. Deep-Sea Res. 35, 767–775.

Crise, A., Crispi, G., Mauri, E., 1998. A seasonal three-dimensional study of the nitrogen cycle in the Mediterranean Sea: Part I. Model implementation and numerical results. J. Mar. Sys. 18, 287–312.

Cruzado, A., 1984. Chemistry of Mediterranean waters. In: Margalef, R. (Ed.), Western Mediterranean. Pergamon, pp. 126–147.

Delgado, M., 1990. Phytoplankton distribution along the Spanish coast of the Alboran Sea. Sci. Mar. 54 (2), 169–178.

Delgado, M., Latasa, M., Estrada, M., 1992. Variability in the size-fractionated distribution of the phytoplankton across the Catalan front of the north–west Mediterranean. J. Plankton Res. 14 (5), 753–771.

Duce, R.A., 1986. The impact of atmospheric nitrogen, phosphorus and iron species on marine biological productivity. In: Buat-Menard, P. (Ed.), The Role of Air–Sea Exchanges in Geochemical Cycles. Reidel, 497–529.

Ducklow, H.W., Purdie, D.A., Williams, P.J.LeB., Davies, J.M., 1986. Bacterioplankton: a sink for carbon in a coastal marine plankton community. Science 232, 865–867.

Eppley, R.W., Peterson, B.J., 1979. Particulate organic matter flux and planktonic new production in the deep ocean. Nature 282, 677–680.

Estrada, M., 1981. Biomasa fitoplanctònica y producciòn primaria en el Mediterràneo occidental, a principio de otoño. Inv. Pesq. 45 (1), 211–230.

Estrada, M., Margalef, R., 1988. Supply of nutrients to the Mediterranean photic zone along a persistent front. Oceanol. Acta 9, 133–142.

Estrada, M., Marrasè, C., Latasa, M., Berdalet, E., Delgado, M., Rieda, T., 1993. Variability of deep chlorophyll maximum characteristics in the northwestern Mediterranean. Mar. Ecol. Prog. Ser. 92, 289–300.

Evans, G.T., Fasham, M.J.R. (Eds.), 1993. Towards a Model of Ocean Biogeochemical Processes. Springer-Verlag, p. 350.

Fabiano, M., Zavatarelli, M., Palmero, S., 1984. Observations sur la matière organique particulaire (protéines, glucides, lipides, chlorophylle) en Mer Ligure. Téthis 11 (2), 133–140.

Fasham, M.J.R., Duklow, H.W., McKelvie, S.M., 1990. A nitrogen-based model of plankton dynamics in the oceanic mixed layer. J. Mar. Res. 48, 591–639.

Garrett, C., 1994. The Mediterranean Sea as a climate test basin. In: Malanotte-Rizzoli, P., Robinson, A. (Eds.), Ocean Processes and Climate Dynamics: Global and Mediterranean Examples. Kluwer, 227–237.

Gould, R.W., Wiesenburg, J.D.A., 1990. Single-species dominance in a subsurface phytoplankton concentration at a Mediterranean Sea front. Limnol. Oceanogr. 35 (1), 211–220.

Heussner, S., Monaco, A., 1995. The MTP sediment trap experiments: highlights on particle fluxes through the eutrophic and oligotrophic systems of the Mediterranean sea. In: Tzelepides, A., Wassman, P. (Eds.), Second Workshop on Mediterranean Targeted Project, 233–238.

Jacques, G., Minas, H.J., Minas, M., Nival, P., 1973. Influence des conditions hivernales sur les productions phyto- et zooplanctoniques en Méditerranée Nord-Occidentale: II. Biomasse et production phytoplanctonique. Mar. Biol. 23, 251–265.

Jacques, G., Minas, M., Neveux, J., Nival, P., Slawyk, G., 1976. Conditiones estivales dans la divergence de Méditerranée Nord-Occidentale: III. Phytoplankton. Ann. Inst. Océanogr. 52 (2), 141–152.

Jacques, G., 1989. Oligotrophie du milieu pelagique de Méditerranée occidentale: un paradigme qui s'estompe?. Bull. Soc. Zoologique de France 114 (3), 17–29.

Jamart, B.M., Winter, D.F., Banse, K., Anderson, G.C., Lam, R.K., 1977. A theoretical study of phytoplankton growth and nutrient distribution in the Pacific Ocean off the nortwestern U.S. coast. Deep-Sea Res. 24, 753–773.

Jamart, B.M., Winter, D.F., Banse, K., 1979. Sensitivity analysis of a mathematical model of phytoplankton growth and nutrient distribution in the Pacific Ocean off the northwestern U.S. coast. J. Plankton Res. 1 (3), 267–281.

Kiefer, D.A., Kremer, J.N., 1981. Origin of vertical patterns of phytoplankton and nutrients in the temperate open ocean: a stratigraphic hypothesis. Deep-Sea Res. A 28 (10), 1087–1105.

Kimor, B., Berman, T., Schneller, A., 1987. Phytoplankton assem-

blages in the deep chlorophyll maximum layers off the Mediterranean coast of Israel. J. Plankton Res. 9 (3), 433–443.
Krom, M.D., Kress, N., Brenner, S., Gordon, L.I., 1991. Phosphorus limitation of primary productivity in the eastern Mediterranean Sea. Limnol. Oceanogr. 36 (3), 424–432.
Krom, M.D., Brenner, S., Kress, N., Neori, A., Gordon, L.I., 1992. Nutrient dynamics and new production in a warm-core eddy from the eastern Mediterranean. Deep-Sea Res. 39, 467–480.
Krom, M.D., Brenner, S., Kress, N., Neori, A., Gordon, L.I., 1993. Nutrient distributions during an annual cycle across a warm-core eddy from the E. Mediterranean Sea. Deep-Sea Res. 40 (4), 805–825.
Lohrenz, S.E., Wiesenburg, D.A., DePalma, I.P., Johnson, K.S., Gustafson, D.E. Jr., 1988. Interrelationships among primary production, chlorophyll, and environmental conditions in frontal regions of the western Mediterranean Sea. Deep-Sea Res. 35 (5), 793–810.
Martin, J.-M., Barth, H. (Eds.), 1995. EROS 2000 (European River Ocean System) Fifth Workshop on the North–West Mediterranean Sea Hamburg (Germany), 28–30 March 1994. Water Pollution Research Report 32, EUR 16130 EN, p. 318.
Minas, H.J., Coste, B., Le Corre, P., Minas, M., Raimbault, P., 1991. Biological and geochemical signatures associated with the water circulation through the Strait of Gibraltar and in the western Alboran Sea. J. Geophys. Res. 96 (C5), 8755–8771.
Pinardi, N., Roether, W., Marshall, J., Lascaratos, A., Krestenitis, Y., Haines, K., 1993. Mediterranean Eddy Resolving Modelling And InterDisciplinary Studies (Contract MAST 0039-C(A)). Final scientific and management Report, p. 45.
Pinazo, C., Marsaleix, P., Millet, B., Estournel, C., Véhil, 1996. Spatial and temporal variability of phytoplankton biomass in upwelling areas of the nortwestern Mediterranean: a coupled physical and biogeochemical modelling approach. J. Mar. Syst. 7, 161–191.
Poulain, P.-M., Gačić, M., Vetrano, A., 1996. Current measurements in the strait of otranto revel unforeseen aspects of its hydrodynamics. EOS Trans. AGU 77 (36), 345–348.
Prieur, L., Sournia, A. (Eds.), 1994. Processes and Fluxes in the Geostrophic Almeria–Oran Front. J. Mar. Syst., Special Issue 5, 3–5, 187–399.
Rabitti, S., Bianchi, F., Boldrin, A., Da Ros, L., Socal, G., Totti, C., 1994. Particulate matter and phytoplankton in the Ionian Sea. Oceanol. Acta 17 (3), 297–307.
Redfield, A.C., Ketchum, B.H., Richards, F.A., 1963. The Influence of Sea Water. In: Hill, M.N. (Ed.), The Sea, Vol. 2. Interscience, New York, 26–77.
Roether, W., Manca, B.B., Klein, B., Bregant, D., Georgopulos, D., Beitzel, V., Kovačević, V., Luchetta, A., 1996. Recent changes in eastern Mediterranean deep waters. Science 271, 333–335.
Roussenov, V., Stanev, E., Artale, V., Pinardi, N., 1995. A seasonal model of the Mediterranean Sea general circulation. J. Geophys. Res. 100 (C7), 13515–13538.
Salihoglu, I., Saydam, C., Basturk, O., Yilmaz, K., Gocmen, D., Hatipoglu, E., Yilmaz, A., 1990. Transport and distribution of nutrients and chlorophyll-*a* by Mesoscale Eddies in the northeastern Mediterranean. Mar. Chem. 29, 375–390.
Sarmiento, J.L., Slater, R.D., Fasham, M.J.R., Ducklow, H.W., Toggweiler, J.R., Evans, G.T., 1993. A seasonal three-dimensional ecosystem model of nutrient cycling in the North Atlantic euphotic zone. Global Biogeochem. Cycles 7 (2), 417–450.
Steele, J.H., Yentsch, C.S., 1960. The vertical distribution of chlorophyll. J. Mar. Biol. Assoc. UK 39, 217–226.
Varela, R.A., Cruzado, A., Tintoré, J., 1994. A simulation analysis of various biological and physical factors influencing the deep chlorophyll maximum structure in oligotrophic areas. J. Mar. Syst. 5, 143–157.
Wassman, P., Tselepides, A. (Eds.), 1995. Second Workshop of the Mediterranean Targeted Project—Extended Abstracts. IMBC-Crete, p. 250.
Wu, P., Haines, K., 1996. Modelling the dispersal of levantine intermediate water and its role in Mediterranean deep water formation. J. Geophys. Res. 101 (C3), 6591–6607.
Yacobi, Y.Z., Zohary, T., Kress, N., Hecht, A., Robarts, R.D., Waiser, M., Wood, A.M., Li, W.K.W., 1995. Chlorophyll distribution throughout the southeastern Mediterranean in relation to the physical structure of the water mass. J. Mar. Syst. 6, 179–190.
Yilmaz, A., Ediger, D., Basturk, O., Tugrul, S., 1994. Phytoplankton fluorescence and deep chlorophyll maxima in northeastern Mediterranean. Oceanol. Acta 17 (1), 69–77.
Zavatarelli, M., Baretta, J., 1996. Three-dimensional ecological model of the Adriatic Sea. Mediterranean Eddy Resolving Modelling And InterDisciplinary Studies-II. Final Scientific and Management Report 1993–1996 (Contract MAS2-CT93-0055), IMGA Research Activity Note 1/1996, 61–64.